A simple synthetic route to obtain pure transruthenium(II) complexes for dye sensitized solar cell applications

A simple synthetic route to obtain pure trans-ruthenium(II) complexes for dye sensitized solar cell applications

Claudia Barolo,[±*][a] Jun-Ho Yum,[±][b] Emma Artuso,[ac] Nadia Barbero,[a] Davide Di Censo,[b] Maria Grazia Lobello,[d] Simona Fantacci,[d] Filippo De Angelis,*[d] Michael Grätzel,[b] Md. K. Nazeeruddin,*[b] and Guido Viscardi[a]

We report a novel, and facile synthetic route to obtain functionalized quaterpyridine ligand and its trans-dithiocyanato ruthenium complex, based on a microwave-assisted procedure. The ruthenium complex has been purified using a silica chromatographic column by protecting carboxylic acid groups as iso-butyl ester, which are subsequently hydrolyzed. The highly pure complex exhibits panchromatic response throughout the visible region. DFT/TDDFT calculations have been performed on the ruthenium complex in solution and adsorbed onto TiO_2 to analyze relative electronic and optical properties. The ruthenium complex endowed with the functionalized quaterpyridine ligand was used as sensitizer in dye sensitized solar cell yielding a short-circuit photocurrent density of more than 19 mA/cm^2 with a broad IPCE spectra ranging from 400 to 900 nm exceeding 80% at 700 nm.

[a] *Dr. C. Barolo, Dr. E. Artuso, Dr. N. Barbero, Prof. G. Viscardi*
Dipartimento di Chimica, NIS Centre of Excellence
Università di Torino
Via Pietro Giuria 7, I-10125, Torino, Italy
Fax: (+)39 011 670 7591
E-mail: claudia.barolo@unito.it

[b] *Dr. J.-H. Yum, Dr. D. Di Censo, Prof. M. Grätzel, Prof. M.K. Nazeeruddin*
Laboratoire de Photonique et Interfaces, Institut des Sciences et Ingénierie Chimiques,
Ecole Polytechnique Fédérale de Lausanne (EPFL)
Station 6, CH-1015, Lausanne, Switzerland
Fax: (+)41 21 6934114
E-mail: mdkhaja.nazeeruddin@epfl.ch

[c] *Dr. E. Artuso*
DYEPOWER
Viale Castro Pretorio 122, 00185 Roma-Italy

[d] *Dr. F. De Angelis, Dr. S. Fantacci, M. G. Lobello*
Istituto CNR di Scienze e Tecnologie Molecolari (ISTM), c/o Dipartimento di Chimica
Università di Perugia
Via Elce di Sotto 8, I-06213, Perugia, Italy
E-mail: filippo@thch.unipg.it

± *These authors contribute equally to the work.*

Introduction

The need to move towards a low carbon economy has led to enormous interest in renewable energy sources, including solar power.[1] Dye-sensitized Solar Cells (DSSCs) provide a technically and economically credible alternative to the conventional p-n junction photovoltaic devices. One of the main components of DSSC's is the mesoporous TiO_2 film, sensitized by a dye monolayer.[2] State of the art DSSCs, based on metallorganic sensitizers, are currently characterized by solar to electric power conversion efficiency of 10-12%.[3]

The prototype solar cells sensitizers are the landmark *cis*-dithiocyanato-4,4'-dicarboxylic acid 2,2′-bipyridyl Ru^{II} (N3), its doubly protonated salt (N719)[4] and the trithiocyanato-4,4',4''-tricarboxylic terpyridyl acid Ru^{II} (N749) complexes. Except from N749[5] and related terpy complexes, the majority of ruthenium complexes reported to date have a *cis* configuration of the NCS ligands, which leads to absorption spectra mainly centered in the visible region at around 535 nm. Therefore, development of new sensitizers with extended absorption spectral sensitivity into the IR region is essential to achieve higher DSSCs photocurrents. [6] By modifying the geometric isomerism of the reported complexes it is possible to obtain variant optical properties,[7] with tailored ligands that stabilize the *trans* configuration. Tetradentate quaterpyridines are suitable ligands for this purpose although they are still largely unexplored.[8] This is likely due to the long synthetic pathway to get these ligands as well as the repeated purification steps required to obtain the pure corresponding metal complexes.[8e-f] Although the highest power conversion efficiency for *trans*-Ru^{II}-complexes was so far only 5.85% (AM 1.5),[8e] attention to this class of dye lies in the possible panchromatic response extending from the NIR to the UV region, rendering them promising alternative sensitizers with enhanced solar harvesting capability over the conventional bipyridyl-based sensitizers. In 2002 a patent [8c] dealing with the synthetic pathway to obtain both the ligand 2,2':6',2'':6'',2'''-quaterpyridine-4,4',4'',4'''-tetracarboxylic acid, **1**, and the corresponding *trans*-complex, **2** and **3**, has been reported, but the synthetic procedures are long and reaction yields are not reported. Particularly, the 2,2':6',2'':6'',2'''-quaterpyridine-4,4',4'',4'''-substituted core was obtained by polymerizing the corresponding pyridine monomer or dimer at reflux for four days in the presence of palladium on carbon. In these cases, the yield of the tetramer derivative is poor and purification is required because large amounts of pyridine dimer/trimer derivatives were also produced. Moreover there are no results concerning the use of the final complex in DSSCs. This lack of information has originally inspired us to seek a new and easy synthetic procedure to obtain the same pure *trans*-complex in order to assess its real potential as a DSSCs sensitizer, serving also as a prototype dye for the subsequent development of new *trans*-Ru^{II}-complexes. Most of the tetradentate ligands were synthetized exploiting various condensation reactions,[9] Kröhnke reaction[8a] or by Stille coupling[8b,e] which led to obtain higher yields in reduced reaction times. Moreover, in recent year[10] microwave-assisted metal-catalyzed C-C bond-forming synthesis has attracted a considerable amount of attention and among Pd-catalyzed cross-coupling a huge number of examples of microwave-assisted Stille reactions has been described in the literature.[10a-b] Recently, the microwave-assisted synthesis of N3 in water has been reported,[11] which allowed to obtain this prototype sensitizer in less time consuming and less labour procedure. Following this trend, we have re-designed the total synthesis of the quaterpyridine ligand **1**, exploiting the above-mentioned microwave-assisted C-C coupling.

Figure 1. Chemical structures of the quaterpyridine ligand **1** and of the corresponding *trans*-Ru^{II} complex in its ester **2**, and acidic form **3**.

In this paper we report a new, easy and reliable microwave-assisted synthetic pathway to the quaterpyridine ligand **1** and the related panchromatic *trans*-Ru^{II} complex **3** (Figure 1) that can be simply transferred to the additional related compounds. Besides DFT/TDDFT study of the *trans*-Ru^{II} complex **3** in solution and adsorbed onto TiO_2 was carried out to clarify the effect of protonation of the terminal carboxylic groups and the dye adsorption mode on the electronic structure, optical and photovoltaic properties respectively.

Results and Discussion

Synthesis

The ligand tetra(*iso*-butyl)-2,2':6',2'':6'',2'''-quaterpyridine-4,4',4'',4'''-tetracarboxylate **1** was obtained as a white solid both under classical (Scheme 1) and microwave conditions (Scheme 2). Both synthetic pathways involve the same intermediates. The key building block bipyridine-bicarboxylate **7** was prepared by a Stille coupling of *iso*-butyl 2-(trimethylstannyl)isonicotinate **5** with *iso*-butyl 2,6-dibromoisonicotinate **6** in dry toluene and the stannyl-derivative **5** was synthesized through a Pd-catalyzed stannylation with hexamethyldistannane of the corresponding *iso*-butyl 2-bromoisonicotinate **4**.

The starting reagents **4** and **6** were prepared from the corresponding methyl isonicotinates by transesterification in *iso*-buthanol (see ESI). Comparing the classical synthetic pathway (Scheme 1) with the microwave-assisted strategy (Scheme 2) it is clear that microwave conditions led to increment of yields and significantly shortened reaction times. The reducing in reaction times is due to our microwave apparatus that allows us to work under pressure at temperatures above the boiling temperature of the reaction solvents. Particularly, for the synthesis of the stannyl-derivative **5** reaction time decreased from 2 h at 110 °C to 4 min at 150 °C under microwave irradiation as well as the yield increased from 79% to 85%. In the case of intermediate **7** the microwave-assisted synthesis allowed to achieve the same yield, but in dramatically reduced time (4 min at 180 °C instead of 24 h at 110 °C). Under classical way (Scheme 1), we obtained ligand **1** in low yield (27%) starting from the corresponding 6-stannyl-derivative **8** and in the presence of the expensive catalyst bis(tri-*tert*-butylphosphine)palladium(0).

Scheme 1. Synthesis of the ligand tetra(*iso*-butyl)-2,2':6',2'':6'',2'''-quaterpyridine-4,4',4'',4'''-tetracarboxylate **1** under classical conditions.

Exploiting microwave irradiation we prepared quaterpyridine **1** through two synthetic pathways (Scheme 2, paths A and B): a one-pot Stille coupling (path A), that without isolating the stannyl-intermediate gave the final ligand in 72% yield after only 8 min, and a C-C direct coupling of the bis(*iso*-butyl)-6-bromo-2,2'-bipyridine-4,4'-bicarboxylate **7** (path B) that in toluene at 200°C for 45 min in the presence of $Pd(CH_3COO)_2$ and DPPP provided ligand **1** in 64% yield. Although the one-pot Stille-approach presented higher yield and shorter reaction time, the homocoupling synthesis only required one reaction step and avoided the use of toxic and unstable stannyl-intermediates.

Scheme 2. Microwave-assisted synthesis of ligand **1**.

Scheme 3. Microwave-assisted synthesis of the *trans*-Ru^{II}-complex **2**.

Table 1. Set up of the microwave-assisted synthesis of the *trans*-Ru^{II}-complex **2** (Scheme 3).

Entry	Ru source	Solvent	Conditions	Yield[a]
1	$[Ru(p\text{-cymene})Cl_2]_2$	DMF	Classical way: (i) 150°C, 4h (ii) 150°C, 16h	20%
2	$[Ru(p\text{-cymene})Cl_2]_2$	DMF	MW: (i) 150°C,30min (ii) 150°C, 3h	39%
3	$[Ru(p\text{-cymene})Cl_2]_2$	EtOH abs	MW: (i) 130°C,30min (ii) 130°C, 2h	14%
4	$RuCl_3$	DMF	MW: (i) 150°C,30min (ii) 150°C, 3h	46%[b]
5	$RuCl_3$	EtOH abs	MW: (i) 130°C,30min (ii) 130°C, 2h	13%[b]

[a] Yields of pure product isolated by column chromatography. [b] MS-ESI^+ spectrum of the final purified complex **2** showed traces of Ru^{III} complex.

The synthesis of the ruthenium complex **3** was accomplished starting from the ligand **1** through the preparation of the Ru^{II}-complex **2** where the carboxylic functionalities have been protected as *iso*-butyl esters (Scheme 3).

This strategy coupled with microwave assisted-synthesis allowed us to get a pure esterified complex **2** and to use conventional silica gel chromatography to purify it.[12]

Initially we set up the microwave-assisted one-pot synthesis of the esterified *trans*-Ru^{II}-complex **2** (Table 1) using different Ruthenium sources and solvents. As shown in Table 1 in all cases microwave irradiation significantly reduced reaction times increasing yields of complex **2**.

Syntheses were carried out both in degassed DMF (Entry 1,2,4) and in absolute ethanol (Entry 3,5), which is cheaper and easier to remove compared with DMF. However, syntheses in absolute ethanol gave complex **2** in lower yields. Starting from $RuCl_3$ we obtained the maximum yield of **2** (Entry 4), unfortunately the purified complex obtained presented a clean ^{1}H-NMR spectrum (Figure 3) but an ESI-MS+ spectrum (see ESI) with a signal at 928 m/z distinctive of a complex containing Ru^{III} instead of Ru^{II}, even if in very low quantity (it was not possible to separate the two complexes by chromatography). Therefore, $[Ru(p\text{-cymene})Cl_2]_2$ was preferred to $RuCl_3$ as a Ruthenium source.

Complex **2** was purified by conventional direct silica-gel chromatography using dichloromethane/acetone 97/3 as an eluent. Finally, pure complex **3** was directly obtained from complex **2** by an easy hydrolysis step carried on with TBAOH 1M water solution (Scheme 4). Only the hydrolysis of the esterified *trans*-Ru(II)-complex **2** obtained in DMF from $[Ru(p\text{-cymene})Cl_2]_2$ (Table 1, Entry 2) led to pure complex **3**.

Scheme 4. Final hydrolysis step to obtain *trans*-Ru^{II}-complex **2**.

NMR Data

^{1}H NMR spectrum of complex **2** purified by silica gel chromatography is reported in Figure 2.

Figure 2. ^{1}H NMR spectrum of purified *trans*-Ru(II)-complex 2 in $CDCl_3$.

Aromatic region shows four signals corresponding to the five pyridyl protons in which the two moieties are magnetically equivalent. This is consistent with an octahedral geometry of the complex where the tetradentate ligand coordinates the metal center in a plane and the isothiocyanate groups are in axial position. Also the ^{13}C NMR (see ESI for details) data are consistent with this interpretation showing no trace of S-coordinated thiocyanate isomers. Figure 3 shows the ^{1}H NMR spectrum of the final dye **3** in [D_6]DMSO. Comparing the integration of the aliphatic signals and the aromatic ones stands it out that each molecule of complex **3** carry about one molecule of TBA.

Figure 3. ^{1}H NMR spectrum of final *trans*-Ru^{II}-complex **3** in [D_6]DMSO.

Electronic structure and spectroscopic properties

The absorption spectrum of the *trans*-Ru^{II}-complex **3** is reported in Figure 4 exhibit two metal-to-ligand charge transfer transitions at 522 and 652 nm, having a molar extinction of 4754 and 5666 mol^{-1} L cm^{-1}, respectively. The lowest-energy band in complex **3** at 652 nm is red-shifted by 130 nm (0.47 eV) when compared to the standard N719 sensitizer (see Figure 4), highlighting the red-shifted response of the *trans*-Ru^{II} complex compared to the prototype *cis*-Ru^{II} N719 complex.

Table 2. Spectroscopic data of complex **3** compared to previously reported trans-Ru^{II} complexes.

	λ_{max} [nm]	ε_{max} [*10^3 $M^{-1}cm^{-1}$]
N886	637	8.3
N1044	615	7.5
Complex 3	652	5.7

Compared to the previously reported trans-Ru(II)-complexes N886[8e] and N1044[8f], endowed, with 4,4'''-tert-butyl and 4,4'''-bis[(E)-2-(3,4-ethylenedioxythienyl)vinyl] substituted quaterpyridine ligands, respectively the complex **3**, substituted by four carboxylic groups, shows 14 nm red-shifted absorption maximum, but with a slightly lower molar extinction coefficient, see Table 2.

To gain insight into the electronic and optical properties of the newly synthesized complex, we performed an extensive Density Functional Theory (DFT)-Time Dependent DFT study of the *trans*-Ru^{II} complex **3** in solution, investigating the effect of protonation of the terminal carboxylic groups on the electronic structure and optical properties of the dyes. Comparing the calculated absorption spectra with the experimental data, allows us to provide a detailed assignment of the UV-vis spectral features of the new complex.

Figure 4. UV-Vis absorption spectra of complex **3** and N719 (normalized absorbance) measured in ethanol solution.

Considering the acidity of the carboxylic groups, we investigated the electronic and optical properties of complex **3** as a function of the protonation state of the ligand. We thus investigated all the possible protonated species of complex **3**, which we label as xH, with x = 4-0 indicating the number of protons carried by the dye. For 3H, 2H and 1H, we have 2, 3 and 2 different tautomers, respectively, see ESI.

Figure 5. Optimized molecular structures of the most stable tautomers of each protonation state of complex **3**. Red circles highlight the position of the protons.

Most of the tautomers are found within less than 1 kcal/mol, so that some mixture of the various species is likely present in solution. For clarity of presentation, from now we will only refer to the most stable tautomers, which are reported in Figure 5.

A schematic molecular orbital energy diagram of investigated complexes is reported in ESI along with isodensity plots of selected molecular orbitals for 3H. The set of quasidegenerate HOMO, HOMO-1 and HOMO-2 of the investigated complexes have essentially Ru t_{2g} character. The LUMOs of the complexes are quaterpyridine π* orbitals, with different electronic localization depending on the pronation pattern. Similar orbital pattern was reported for the tetra-protonated complex **3** by Pan et al.[13] The main difference occurring with deprotonation is an opening of the HOMO-LUMO gap from 2.27 to 2.74 eV, going from 4H to 0H, due to a larger destabilization of the unoccupied with respect to the occupied orbitals. The ester derivative **2** shows a similar electronic structure to that of the tetraprotonated complex **3**, see ESI.

The calculated absorption spectra and the most representative calculated optical transitions for all the considered species are reported in ESI. In all cases the main absorption features of the experimental spectrum are well reproduced by theory. Varying the degree of protonation from 4H to 0H, the longest wavelength absorption maximum is blue shifted from 758 nm to 601. The calculated absorption spectrum of 3H is the one, which better agrees with the experimental one, see a comparison of calculated and experimental spectra in Figure 6.

For the 3H species, the first band, experimentally found at 652 nm, is computed at 708 nm, only 0.15 eV red-shifted with respect to the experimental data, and appears to be composed of two transitions at 764 and 701 nm, which originated from the HOMO-1/HOMO (Ru-SCN) couple to the LUMO (π* on pyridines), see ESI.

The second band, experimentally found at 522 nm, is computed at 526 nm only 0.02 eV red-shifted with respect to the experimental data, and is composed by four transitions at 581, 546, 523 and 501 nm, which originated from the HOMO-1/HOMO (Ru-SCN) couple to the LUMO+1/LUMO+2 (π* on pyridines). In both cases we assign the transitions as having MLCT character.

Figure 6. Comparison between the simulated spectrum of 3_3H (red line) and the experimental spectrum (green line). Vertical red lines correspond to calculated excitation energies and oscillator strengths.

The band in UV region computed at 363 nm is assigned as of mixed character, being constituted by MLCT and π → π* contributions. It is also interesting to notice that for 3H we calculate a molar extinction coefficient for the longest wavelength band of 6081 mol^{-1} L cm^{-1}, in excellent agreement with the experimental value of 5666 mol^{-1} L cm^{-1}. Thus, although we cannot exclude the presence of different tautomers, our results seem to suggest that the species carrying three protons could dominate the solution equilibrium.

To gain insight into the adsorption mode of complex **3** onto TiO_2, we optimized the structure of the 3H species anchored to a $(TiO_2)_{82}$ anatase cluster exposing (101) faces.[14] As previously reported,[8f] the adsorption mode is characterized a bridged bidentate carboxylic group and by a dissociated monodentate carboxylic group, see ESI. Thus the IR signature of this adsorption mode is expected to show the typical spectroscopic pattern of the two different carboxylic groups, with asymmetric and symmetric stretching typical of the bridged bidentate mode at ca. 1550 and 1430 cm^{-1} and a higher energy peak corresponding to the unbound carboxylate C=O stretching. This hypothesis, solely based on the calculated structure, has been also verified on the base of the FT-IR data shown below.

We then calculated the electronic structure and TDDFT absorption spectrum of complex 3-3H on TiO_2. A survey of this data is reported in Figure 7, where we show the calculated lowest absorption band for the dye on TiO_2 and selected LUMOs.

Figure 7. Calculated LUMOs for complex **3** adsorbed onto TiO_2 (upper left, bottom left and right panels) and TDDFT absorption spectrum of the lowest energy band for 3@TiO_2 (upper right panel).

The calculated absorption spectrum for **3**@TiO_2 shows a lowest energy absorption maximum at 704 nm, i.e. very similar to the corresponding value in solution. The transitions characterizing the lowest energy band all involve excitation to the LUMO+1 and LUMO+2 states, which have sizable components from the dye π* orbitals, mixed with TiO_2 unoccupied states. Considering the low-lying dye LUMO, compared to the TiO_2 conduction band edge, some problems with electron injection can be anticipated.

In order to elucidate the characteristic of the surface attachment of the dye ATR spectra of both dye alone and dyed electrode were performed (Figure 8).

The NCS^- group has two characteristic modes, *υ*(NC) and *υ*(CS), which are frequently considered as diagnostic with respect to the coordination mode of the ambidentate NCS ligand.[15] The IR spectrum of complex **3** shows an intense absorbance at 2120 *υ*(NC) and 780 *υ*(CS) cm^{-1} due to the N-coordinated NCS ligand. The two sets of bands at 1709 and 1652 cm^{-1} in complex **3** are due to the presence of protonated and deprotonated carboxyl groups. The comparison between the two spectra shows that the C=O peak at 1709 cm^{-1} decrease dramatically when the dye is absorbed on titania surface, while is growing the peak at 1652 cm^{-1} due to the C=O of carboxylate species.

Concerning the binding mode of the carboxylic groups on the titania surface we can recognize the presence in the spectrum of the asymmetric and symmetric stretching typical of the bridged bidentate mode at 1541 and 1419 cm^{-1} (see also data from calculated structure) and a higher energy peaks corresponding to ν^{COO}_{asym} for the monodentate anchoring mode and the unbound carboxylate C=O stretching.[8f] The difficulty in identifying a particular configuration is also due to the presence in the experimental spectrum of unspecific signals, such as ring modes, that overlap with potentially revealing signals.[16]

Figure 8. Comparison between the ATR spectrum of Complex **3** powder (red line) and the ATR spectrum of Complex 3 absorbed on TiO_2 (blu line).

Electrochemical properties

The electrochemical characterization of the complexes **3** and **2** was carried out on a glassy carbon electrode using Cyclic Voltammetry (CV, Figure 9). Species **3** has protonated carboxy-groups, which can reduce at the same time as the ligands and shows poor reversibility of its redox processes. In this regard data relative to species **2** (i.e. with esters in place of carboxy groups) and MO calculations were used to reduce ambiguities in the interpretation of the voltammetry. Measurements of the oxidation potential provide information about the ground state oxidation potential of the complexes in solution. The two complexes show the same formal potential for the oxidation process, E°' 0.50 V vs Fc^+/Fc (which gives 1.16 V vs NHE considering the redox couple Fc^+/Fc to be located at 0.66 V vs NHE). This is in accordance with the MO calculation showing a very close position of the HOMO, i.e. -5.63 and -5.64 eV respectively.

Figure 9. CV of complexes **3** (with Ferrocene added as internal standard) and complex **2** carried out at 1V/s on a glassy carbon electrode, 2nd scan is showed.

The formal potentials for the reduction of the complexes **3** and **2** are observed at -1.35 and -1.27 V vs Fc^+/Fc, respectively (which gives -0.69 and -0.61 V vs NHE considering the redox couple Fc^+/Fc to be located at 0.66 V vs NHE). This reduction process can be associated with an e^- transfer to the π* orbitals on the quaterpyridine, it shows quasi reversibility, as given by observing the peak-to-peak separation and intensity. The formal reduction potential can be used as an estimation of the LUMO energy. Another estimation of

the LUMO level for **3** can be obtained by subtracting the value of the optical band gap from the value of the oxidation potential. This method provides the LUMO of the dye located at even lower levels (-0.45 V vs NHE for complex **3**).

In the case of **3** a larger deviation of the baseline of CV is observed, that can be related to a competitive reduction of the protons on carboxylic acid group. The 80 mV difference observed between complexes **3** and **2** is consistent with the calculations showing position of the LUMO at -3.32 eV and -3.42 eV respectively.

Photovoltaic properties[17]

Dye sensitized solar cells were fabricated by adsorbing complex **3** onto a TiO_2 film of 12 µm thickness, made of ~20 nm anatase nanoparticles. An electrolyte composed of 1.0 M of dimethylimidazolium iodide, 0.03 M of iodine, 0.1 M of 3α,7α-dihydroxy-5β-cholic acid, and 0.1 M of guanidinium thiocyanate was used, employing a variable amount of added LiI in the concentration range 0.10-0.23 M. The photovoltaic performances were measured at 1 sun under AM 1.5 conditions. Table 3 presents photovoltaic results with various LiI concentrations, while Figure 10 shows the current/voltage characteristics.

Figure 10. Photovoltaic data of complex **3** as a function of LiI concentration and in the presence of co-sensitization by D35. Dotted lines indicate dark currents of devices.

The best cell efficiency under full sun is 6.53% with a short circuit current density (Jsc) exceeding 19 mA/cm^2. Unfortunately the rather low open circuit potential (Voc), 557 mV, penalties the overall cell performance.

Table 3. Photovoltaic data of complex **3** obtained under different LiI concentration and in the presence of co-sensitization by the D35 dye.

Li concentration	J_{sc} [mAcm^{-2}]	V_{oc} [mV]	FF	Eff. [%]
0.10M	17.6	564	0.64	6.36
0.17M	18.1	551	0.65	6.45
0.23M	19.1	548	0.62	6.53
0.23M[a]	19.8	557	0.63	6.88

[a] Co-sensitized with D35

Additives in an electrolyte are known to influence on a DSSC cell performance15c and the relatively high concentration of Li^+ and no 4-tert-butylpyridine in this study plausibly resulted in the low Voc.

Indeed, the Jsc and Voc are dependent on LiI concentration as shown in Table 3, where the higher concentration of Li^+ lowers the TiO_2 conduction band thereby facilitating high charge injection finally leading to an increase in Jsc at the cost of a Voc decrease. Beyond the effect of added LiI, the low Voc might also due to parasitic recombination reactions involving TiO_2 injected electrons and the oxidized dye and/or oxidized species in the electrolyte. This behavior was repeatedly found for related trans-Ru^{II} complexes,[8e-f] see Table 4.

Table 4. Photovoltaic data of complex **3** compared to previously reported *trans*-Ru^{II} complexes

	J_{sc} [mAcm^{-2}]	V_{oc} [mV]	FF	Eff. [%]
N886	11.8	680	0.73	5.85[7e]
N1044	19.2	447	0.67	5.7[7f]
Complex 3	19.1	548	0.62	6.53

Figure 11 presents the incident photon to current conversion efficiency (IPCE) spectrum plotted as function wavelength from 400 to 900 nm for the best performing cell. It is striking to observe the high IPCE value at 700 nm, which exceeds 80%. Only some tertpyridyl ruthenium complexes[5,18] have shown such a high IPCEs at red/NIR region, however no comparable result has been reported in quarterpyridyl ruthenium complex; for example DSSCs fabricated with the N1044 dye (whereas quaterpyridine skeleton have been decorated with EDOT moieties) exhibited ca. 60% IPCE at 700 nm.

Figure 11. IPCE spectra of DSSCs based on complex **3** without (black solid line) and with D35 (red dashed line). LiI 0.23 M.

It is also interesting to notice that while N1044 showed an almost constant IPCE up to ca. 400 nm, in the present case the IPCE shows a steady decrease above 500 nm, reflecting the diminishing absorption intensity in this wavelength region (see Figure 4 and 11).

Obviously, the reduced IPCE at around 500 nm leads to a reduction of the Jsc, therefore co-sensitization[19] with the D35 organic dye,[20] that shows complementary spectral responses in the 500 nm region, was used to improve even more the light harvesting characteristics of the cell. As a result, the device performance increased to 6.9% mainly due to an increase in Jsc close to 20 mA/cm^2 and the IPCE spectrum of the co-sensitized device showed a dramatic increase in the spectral region of 400 – 630 nm.

Conclusion

Herein, we present a new reliable and easy microwave-assisted synthetic pathway to prepare a highly pure quaterpyridine ligand and the corresponding *trans*-Ru^{II} complexes in good yield. The use of hydrophobic protective ester functionalities for carboxylic acid groups allowed to apply silica based chromatographic techniques in purification step of intermediate complex, whose quantitative hydrolysis of intermediate complex allowed to obtain final *trans*-Ru^{II} complex in required purity level. *Trans*-Ru^{II} complex is panchromatic having an IPCE ranging from 400 to 900 nm and shows an overall photovoltaic conversion efficiency of 6.53% at standard AM 1.5 sunlight, that is the best efficiency reported up to now for tetradentate ligand-based Ru^{II} complexes. Further molecular engineering on this class of sensitizers to increase molar extinction coefficient and shift the LUMO level to increase Voc would enhance overall performance of the cell.

Experimental Section

Materials and methods

^{1}H NMR and ^{13}C NMR spectra were recorded on a Bruker Avance-200. ESI-MS spectra were recorded using a LCQ Deca XP plus spectrometer (Thermo) spectrometer with electrospray interface and ion trap as a mass analyzer; sheath gas flow rate is set at 25 (arbitrary unit), auxiliary gas flow rate at 5 (arbitrary unit), spray voltage at 3.25 (KV), capillary temperature at 270 °C, capillary voltage at −7 (V), and tube lens offset at −60.00 (V). Nitrogen is used as a sheath and auxiliary gas. High-resolution data were recorded on an LTQ Orbitrap Hybrid Mass Spectrometer.

All the chemicals were purchased from Sigma-Aldrich and were used as received unless stated otherwise. Column chromatography purifications were performed by classical chromatography using silica gel (Merck Grade 7734, pore size 60 Å, 70-230 mesh).

The glassware used for classical syntheses was heated overnight in an oven at 150°C and assembled in the oven, then cooled under argon flux before starting the reactions.

Microwave-assisted reactions were carried out by a Biotage Initiator EXP synthesizer. Reactions were conducted in Biotage microwave vials which were loaded under argon atmosphere using dried and degassed solvents.

Syntheses

General microwave-assisted synthesis of tetra(*iso*-butyl)-2,2':6',2'':6'',2'''-quaterpyridine-4,4',4'',4'''-tetracarboxylate **1** (homocoupling): A microwave vial was charged with di*iso*-butyl 6-bromo-2,2'-bipyridine-4,4''-dicarboxylate **7** (35.0 mg, 0.080 mmol), $Pd(CH_3COO)_2$ (2.0 mg, 8.9*10^{-3} mmol), 1,3-bis(diphenylphosphino)propane (DPPP, 2.4 mg, 5.6*10^{-3} mmol) and Cs_2CO_3 (35.0 mg, 0.100 mmol). Then the vial was closed and filled with Argon. Afterwards, degassed anhydrous toluene (1.00 ml) was added and the resulting reaction mixture was further degassed with argon for 15 min. The mixture was heated by microwave irradiation at 200 °C for 45 min (the reaction was monitored by MS-ESI$^+$). The reaction mixture was diluted with dichloromethane, filtered through a pad of celite with copious washing (dichloromethane) and concentrated under vacuum. The resulting residue was purified by silica gel column chromatography eluting with PE/ethyl acetate 80/20 to yield 18 mg (64%) of the desired compound. ^{1}H NMR (200 MHz, $CDCl_3$, 25 °C, TMS): δ=9.2 (d, ^3J(H,H)=2 Hz, 2H; $H_{3'}$+$H_{5''}$), 9.2 (m, 2H; $H_{5'}$+$H_{3''}$), 9.1 (d, ^3J(H,H)=2 Hz, 2H; H_3+$H_{3'''}$), 8.9 (dd, ^3J(H,H)=2 Hz, ^3J(H,H)=4 Hz, 2H; H_6+$H_{6'''}$), 7.9 (dd, ^3J(H,H)=2 Hz, ^3J(H,H)=4 Hz, 2H, H_5+$H_{5'''}$), 4.2 (m, 8H; 4xCH_2, O-CH_2CH(CH_3)$_2$), 2.2 (m, 4H; O-CH_2CH(CH_3)$_2$), 1.1 ppm (dd, ^3J(H,H)=2 Hz, ^3J(H,H)=6 Hz, 24H; O-CH_2CH(CH_3)$_2$). ^{13}C NMR (50 MHz, $CDCl_3$, 25 °C): δ=165.0, 156.1, 149.8, 139.6, 120.8, 71.7, 27,2, 19.0 ppm. HR-MS (ESI) m/z calcd for (C40H46N4O8): 710.8152. Found: 711.3444.

General microwave-assisted synthesis of trans-[Ru(i-Bu_4-2,2':6',2'':6'',2'''-quaterpyridine-4,4',4'',4'''-tetracarboxylate)$(NCS)_2$] **2**: A microwave vial was charged with the ligand tetra(*iso*-butyl)-2,2':6',2'':6'',2'''-quaterpyridine-4,4',4'',4'''-tetracarboxylate **1** (40.0 mg, 0.0563 mmol) and the ruthenium source [Ru(p-cymene)Cl_2]$_2$ (17.3 mg, 0.0282 mmol) or $RuCl_3$ 45% (26.0 mg, 0.0563 mmol). The vial was closed and filled with Argon. Afterwards, solvent (degassed DMF or degassed ethanol, 17.0 ml) was added by a syringe and the resulting reaction mixture was further degassed with argon for 15 min. The vial was heated by microwave for 30 min with stirring at 130 °C for reactions in ethanol or at 150 °C for reactions in DMF (reaction was monitored by ESI-MS$^+$ until disappearance of the starting quaterpyridine signal). After this time the vial was opened and ammonium thiocyanate (500 mg) was added. The vial was again closed and the reaction mixture degassed with argon for 15 min. The second step was carried out at temperature and time indicated in Scheme 3. The solvent was evaporated under vacuum and the resulting residue was purified by classical silica gel chromatography eluting with dichloromethane/acetone 97/3. Complex **2** was the first fraction and was obtained as a dark green solid. The yields of the reactions are reported in Scheme 3.

See Supporting Information for detailed both classical and microwave-assisted syntheses of intermediates and results of ^{1}H and ^{13}C NMR spectroscopy.

Computational

We optimized the geometries of the dye-adsorbed structure using a DZ basis set and the PBE functional,[21] as implemented in the ADF code.[22] No simplifications in the dye structure were made. On the optimized geometries we performed single point energy evaluations and Time Dependent DFT (TDDFT) excited state calculations using the B3LYP functional[23] and a 3-21G* basis set, including solvation effects by the C-PCM model,[24] as implemented in the Gaussian 09 program package.[25] For the study of dyes in solution we used the B3LYP functional and a 3-21G* basis set for geometry optimization followed by TDDFT calculations using a larger DGDZVP basis set.

Electrochemical Characterization

Voltammetric measurements employed a PC controlled AutoLab PSTAT10 electrochemical workstation and were carried out in an Ar-filled glove box, oxygen and water < 1 ppm. Cyclic Voltammetry and Differential Pulse Voltammetry techniques were used to estimate the redox potentials. CVs were obtained at a scan rate of 1 Vs^{-1}. Measurements were carried out using 0.1 M $HPPPF_6$ as supporting electrolyte in dimethylformamide (DMF). Glassy carbon, platinum plate and platinum wire were as working, counter and quasi-reference electrodes, respectively. At the end of each measurement, ferrocene was added as internal reference. We have considered the redox couple Fc+/Fc to be located at 0.66 V vs NHE in DMF.

Solar Cell Fabrication and Characterization

The nanocrystalline TiO_2 pastes were prepared using a previously reported procedure.[10] The TiO_2 transparent electrodes composed of ~20 nm anatase on fluorine doped thin oxide (FTO, Solar 4 mm thickness, 10 ohms/sq, Nippon Sheet Glass, Japan) conducting glass were controlled to be ~12 µm by the number of screen printing passes. In order to render high power conversion efficiency, a ~5 µm scattering layer (400 nm diameter, CCIC, HPW-400) was deposited on the transparent layer. The TiO_2 electrodes were immersed into a 0.18 mM solution of complex 3 in 4-*tert*-butanol/acetonitrile mixture (1:1 v/v) containing 10% dimethylformamide (DMF) and kept for overnight at room temperature. For cosensitization, 0.05 M D35 was added into the complex 3 solution. The applied electrolyte consists of 1.0 M 1,3-dimethylimidazolium iodide (DMII), 0.03 M iodine, 0.1 M guanidinium thiocyanate, 0.1 M 3α,7α-dihydroxy-5β-cholic acid and LiI ranging from 0.1 M to 0.23 M in 15/85 (v/v) mixture of valeronitrile and acetonitrile. The dye-adsorbed TiO_2 electrode and thermally platinized counter electrode or PProDOT counter electrode on FTO (TEC 15 ohms/sq, Pilkington) were assembled into a sealed sandwich type cell with a gap of a hot-melt ionomer film, Surlyn (25 µm, Du-Pont). A self-adhesive, anti-reflecting, UV cut-off film (λ < 380 nm, ARKTOP, ASAHI Glass) was attached to the top of active area to decrease light reflection loss. For photovoltaic measurements of the DSCs, the irradiation source was a 450 W xenon light source (Osram XBO 450, Germany) with a filter (Schott 113), whose power was regulated to the AM 1.5G solar standard by using a reference Si photodiode equipped with a colour matched filter (KG-3, Schott) in order to reduce the mismatch in the region of 350-750 nm between the simulated light and AM 1.5G to less than 4%. The measurement settling time between applying a voltage and measuring a current for the *J-V* characterization of DSCs was fixed to 40 ms. The incident photon to collected electron conversion efficiency (IPCE) measurement was plotted as function of wavelength by using the light from a 300 W xenon lamp (ILC Technology, USA), which was focused through a Gemini-180 double monochromator (Jobin Yvon Ltd., UK) onto the photovoltaic cell under test. A computer controlled monochromator was incremented through the spectral range (340-1000 nm) to generate a photocurrent action spectrum with a sampling interval of 10 nm and a current sampling time of 4 s. In order to reduce scattered light from the edge of the glass electrodes of the dyed TiO_2 layer, a light shading mask was used on the DSCs, so the active area of DSCs was fixed to 0.2 cm^2.

Acknowledgements

Authors acknowledge financial support by FP7-NMP-2009 project SANS (246124) and FP7-ENERGY-2010 project ESCORT (261920). M.K.N. acknowledges financial support by FP7-NMP-2008 project ORION (229036). S.F. and G.V. gratefully acknowledge financial support by DSSCX project (PRIN 2010-2011, 20104XET32) from Ministero dell'Istruzione, dell'Università e della Ricerca. NB thanks MIUR for partial financial support of her Research grant. CB thanks the Balzan Foundation for partial financial support as part of the 2009 Balzan Prize awarded to MG. M.K.N. thanks the World Class University program funded by the Ministry of Education, Science and Technology through the National Research Foundation of Korea (R31-2011-000-10035-0), Department of Materials Chemistry, Korea University.

Keywords: quaterpyridine ligands · *trans*-Ru^{II} complexes· microwave-assisted syntheses· ruthenium sensitizers· Dye-Sensitized Solar Cells

[1] N. Murakami-Iha, C.G. Garcia, C.A. Bignozzi, *Handbook of Photochemistry and Photobiology*, Nalwa H.S. **2003**, *1*, p.49.

[2] a) B. Li, L.D. Wang, B.N. Kang, P. Wang, Y. Qiu, *Sol. Energy Mater. Sol. Cells* **2006**, *90*, 549-573; b) B.C. O'Regan, M. Grätzel, *Nature* **1991**, *353*, 737-740.

[3] a) A. Yella, H.-W. Lee, H. Nok Tsao, C. Yi, A. K. Chandiran, Md.K. Nazeeruddin, E. Wei-Guang Diau, C.-Y. Yeh, S. M Zakeeruddin, M. Grätzel, *Science* **2011**, *334,* 629-634; b) F. Sauvage, D. Chen, P. Comte, F. Huang, L.-P. Heiniger, Y.-B. Cheng, R. A. Caruso, M. Grätzel, *ACS Nano* **2010**, *4*, 4420-4425; c) C.-Y. Chen, M. Wang, J.-Y. Li, N. Pootrakulchote, L. Alibabaei, C. Ngoc-le, J.-D. Decoppet, J.-H. Tsai, C. Grätzel, C.-G. Wu, S. M. Zakeeruddin, M. Grätzel, *ACS Nano* **2009**, *3*, 3103-3109; d) F. Sauvage, J. D. Decoppet, M. Zhang, S. M. Zakeeruddin, P. Comte, Md. K. Nazeeruddin, P. Wang, M. Grätzel, *J. Am. Chem. Soc.* **2011**, *133*, 9304-9310; e) F. Gao, Y. Wang, D. Shi, J. Zhang, M. Wang, X. Jing, R. Humphry-Baker, P. Wang, S. M. Zakeeruddin, M. Grätzel, *J. Am.*

Chem. Soc. **2008**, *130*, 10720-10728; f) Y. Cao, Y. Bai, Q. Yu, Y. Cheng, S. Liu, D. Shi, F. Gao, P. Wang, *J. Phys. Chem. C* **2009**, *113*, 6290-6297; g) L. Han, A. Islam, H. Chen, C. Malapaka, B. Chiranjeevi, S. Zhang, X. Yang, M. Yanagida, *Energy Environ. Sci.*, **2012**, *5*, 6057-6060.

[4] a) M.K. Nazeeruddin, F. De Angelis, S. Fantacci, A. Selloni, G. Viscardi, P. Liska, S. Ito, B. Takeru, M. Grätzel, *J. Am. Chem. Soc.* **2005**, *127*, 16835-16847; b) R. Buscaino, C. Baiocchi, C. Barolo, C. Medana, M. Grätzel, M. K. Nazeeruddin, G. Viscardi, *Inorg. Chim. Acta* **2008**, *361 (3)*, 798-805.

[5] M.K. Nazeeruddin, P. Péchy, T. Renouard, S.M. Zakeeruddin, R. Humpry-Baker, P. Compte, P. Liska, L. Cevey, E. Costa, V. Shklover, L. Spiccia, G.B. Deacon, C.A. Bignozzi, M. Grätzel, *J. Am. Chem. Soc.* **2001**, *123,* 1613-1624; b) S. Fantacci, M.G. Lobello, F. De Angelis, *Chimia* **2013**, 67 (3),121-128.

[6] J. Park, G. Viscardi, C. Barolo, N. Barbero, *Chimia* **2013**, 67 (3), 129-135.

[7] M.K. Nazeeruddin, S.M. Zakeeruddin, R. Humpry-Baker, S.I. Gorelsky, A.B.P. Lever, M. Grätzel, *Coord. Chem. Rev.* **2000**, *208*, 213-226.

[8] a) T. Renouard, M. Grätzel, *Tetrahedron* **2001**, *57*, 8145-8150; b) T. Renouard, R.A. Fallahpuor, M.K. Nazeeruddin, R. Humphry-Baker, S.I. Gorelsky, A.B.P. Lever, M. Grätzel *Inorg. Chem.* **2002**, *41 (2)*, 367-378; c) R.Y. Paidi, M. Ito (Aisin Seiki), US-B1 6437130, **2002**; d) A. Islam, L. Han, A. Fukui (Sharp), US-A1 139257, **2005**; e) C. Barolo, M.K. Nazeeruddin, S. Fantacci, D. Di Censo, S. Ito, P. Comte, P. Lisk, G. Viscardi, P. Quagliotto, F. De Angelis, M. Grätzel, *Inorg. Chem.* **2006**, *45*, 4642-4653; f) A. Abbotto, F. Sauvage, C. Barolo, F. De Angelis, S. Fantacci, M. Grätzel, N. Manfredi, C. Marinzi, M.K. Nazeeruddin, *Dalton Trans.* **2011**, *40*, 234-242.

[9] a) K. Mizuschimam, N. Nakaura, S.B. Park, H. Nishiyama, H. Manjushira, K. Harada, M. Haga, *Inorg. Chim. Acta* **1997**, *261*, 175-180; b) T. Renouard, M. Grätzel, *Tetrahedron* **2001**, *57*, 8145-8150.

[10] a) C.O. Kappe, *Angew. Chem. Int. Ed.* **2004**, *43*, 6250-6284; b) V. P. Mehta, E. V. Van der Eycken, *Chem. Soc. Rev*. **2011**, *40*, 4925-4936.

[11] a) S. H. Kristensen, J. Toster, K. S. Iyer, C. L. Raston, *New J. Chem.* **2011**, *35*, 2752-2754; b) R. Boaretto, E. Busatto, S. Carli, S. Fracasso, S. Caramori, C. A. Bignozzi (DyePower), WO-A1 073268, **2012**.

[12] T. Rawling, F. Buchhloz, A.M. McDonagh, *Aust. J. Chem*. **2008**, *61*, 405-408.

[13] Qing-Jiang Pan, Yuan-Ru Guo, Li Li, Samuel O. Odoh, Hong-Gang Fu, Hong-Xing Zhang, *Phys. Chem. Chem. Phys.* **2011**, *13*, 14481-14490.

[14] F. De Angelis, S. Fantacci, A. Selloni, M. K. Nazeeruddin, M. Grätzel, *J. Phys. Chem. C* **2010**, *114*, 6054-6061.

[15] S. Wajda, K. Rachlewicz, *Inorg. Chim. Acta* **1978**, *31*, 35-40.

[16] F. Schiffmann, J. VandeVondele,J. Hutter, R. Wirz, A. Urakawa, A. Baiker *J. Phys Chem. C* **2010**, *114*, 8398-8404.

[17] a) S. Nakade, T. Kanzaki, W. Kubo, T. Kitamura, Y. Wada, S. Yanagida, *J. Phys. Chem. B* **2005**, *109*, 3480-3487; b) G. Boschloo, L. Häggman, A. Hagfeldet, *J. Phys. Chem. B* **2006**, *110*, 13144-13150; c) S. E. Koops, B.C. O'Regan, P.R.F. Barnes, J.R. Durrant, *J. Am. Chem. Soc.* **2009**, *131*, 4808-4818.

[18] a) N. Onozawa-Komatsuzaki, M. Yanagida, T. Funaki, K. Kasuga, K. Sayama, H. Sugihara, *Inorg. Chem. Commun.* **2009**, *12*, 1212-1215; b) T. Funaki, M. Yanagida, N. Onozawa-Komatsuzaki, K. Kasuga, Y. Kawanishi, H. Sugihara, *Chem. Lett.* **2009**, *38*, 62-63.

[19] J.H. Yum, E. Baranoff, S. Wenger, Md. K. Nazeeruddin, M. Grätzel, *Energy Environ. Sci.* **2011**, *4*, 842-857.

[20] D.P. Hagberg, X. Jiang, E. Gabrielsson, M. Linder, T. Marinado, T. Brinck, A. Hagfeldt, L. Sun, *J. Mater. Chem.* **2009**, *19*, 7232-7238.

[21] J.P. Perdew, K. Burke, M. Ernzerhof, *Phys. Rev. Lett.* **1996**, 77, 3865-3868.

[22] G. Velde, F. M. Bickelhaupt, E. J. Baerends, C. Fonseca Guerra, S. J. A. Van Gisbergen, J. G. Snijders, T. J. Ziegler, *Comput. Chem.* **2001**, *22*, 931-967.

[23] A. D. J. Becke, *Chem. Phys.* **1993**, *98*, 5648-5652.

[24] a) M. Cossi, V. Barone, *J. Chem. Phys.* **2001**, *115*, 4708-4717; b) M. Cossi, N. Rega, G. Scalmani, V. Barone, *J. Comp. Chem.* **2003**, *24*, 669-681.

[25] Gaussian 09 (Revision A.01): M. J. Frisch et al. see Supporting Information.

Graphics

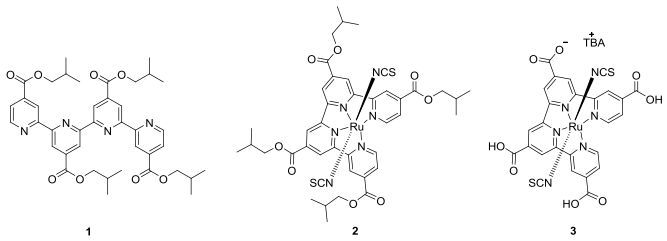

Figure 1. Chemical structures of the quaterpyridine ligand **1** and of the corresponding *trans*-Ru^{II} complex in its ester **2**, and acidic form **3**.

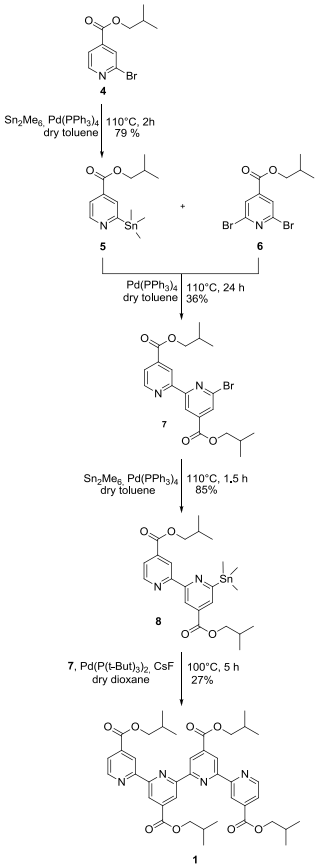

Scheme 1. Synthesis of the ligand tetra(*iso*-butyl)-2,2':6',2'':6'',2'''-quaterpyridine-4,4',4'',4'''-tetracarboxylate **1** under classical conditions.

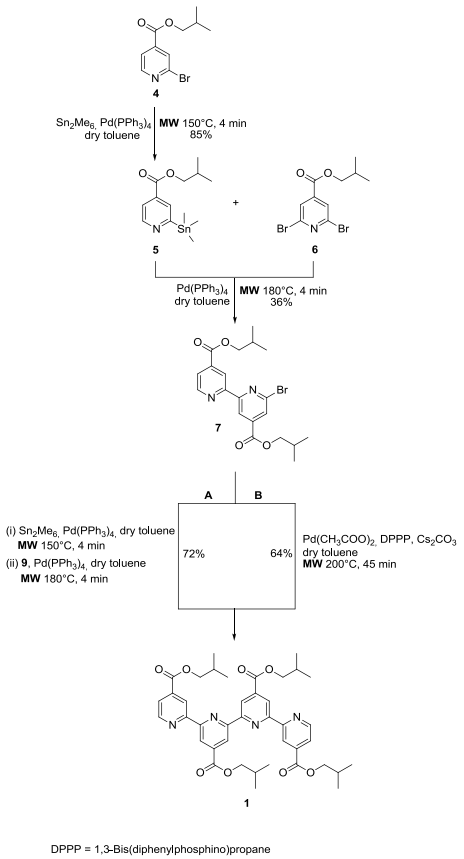

Scheme 2. Microwave-assisted synthesis of ligand **1**.

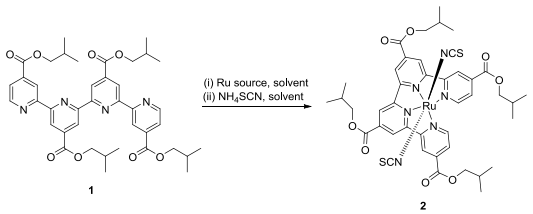

Scheme 3. Microwave-assisted synthesis of the *trans*-Ru^{II}-complex **2**.

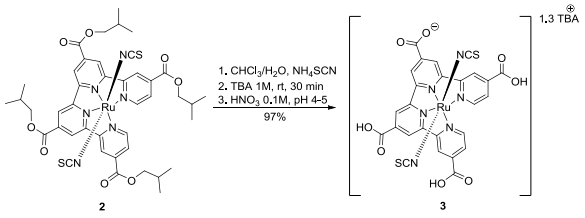

Scheme 4. Final hydrolysis step to obtain *trans*-Ru^{II}-complex **2**.

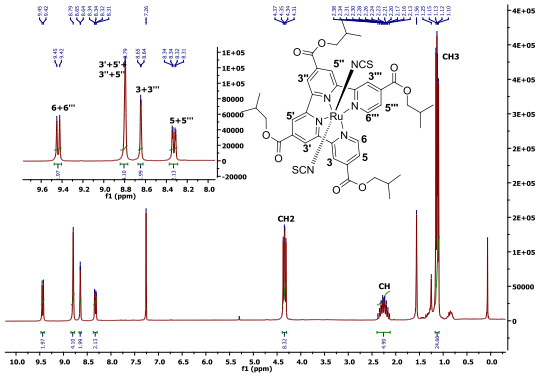

Figure 2. ^{1}H NMR spectrum of purified *trans*-Ru(II)-complex 2 in $CDCl_3$.

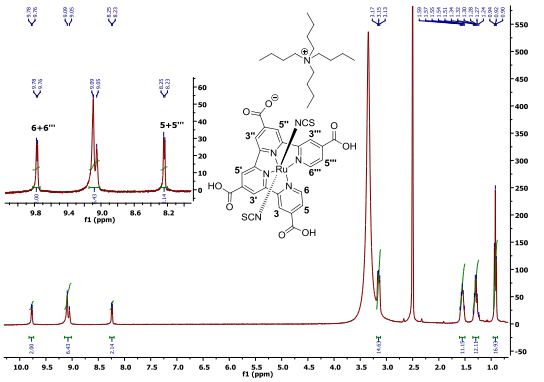

Figure 3. ^{1}H NMR spectrum of final *trans*-Ru^{II}-complex **3** in $[D_6]$DMSO.

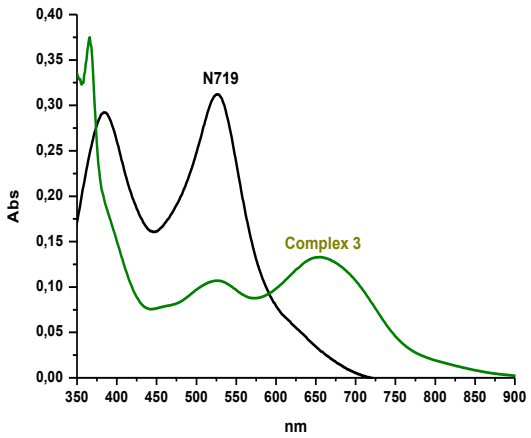

Figure 4. UV-Vis absorption spectra of complex **3** and N719 (normalized absorbance) measured in ethanol solution.

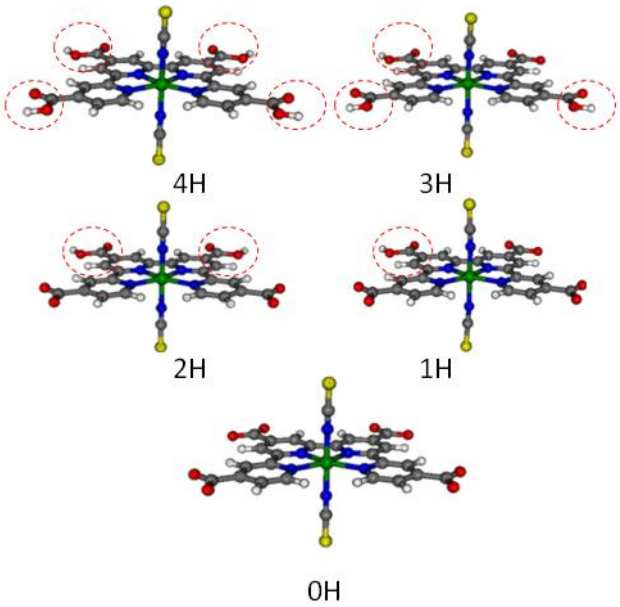

Figure 5. Optimized molecular structures of the most stable tautomers of each protonation state of complex **3**. Red circles highlight the position of the protons.

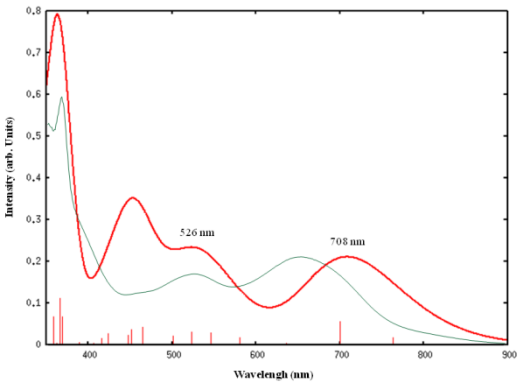

Figure 6. Comparison between the simulated spectrum of 3_3H (red line) and the experimental spectrum (green line). Vertical red lines correspond to calculated excitation energies and oscillator strengths.

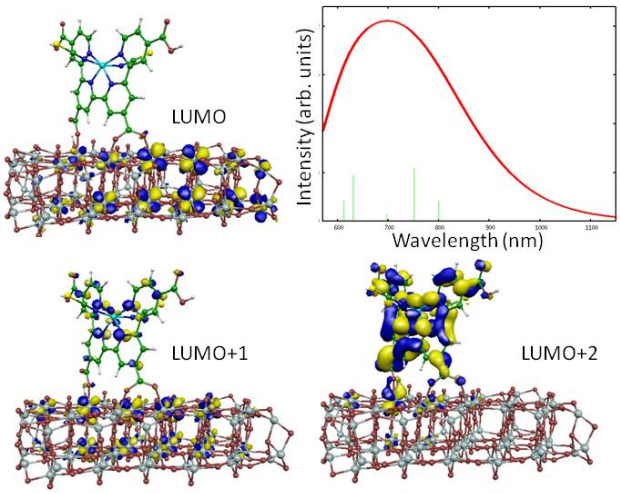

Figure 7. Calculated LUMOs for complex **3** adsorbed onto TiO_2 (upper left, bottom left and right panels) and TDDFT absorption spectrum of the lowest energy band for 3@TiO_2 (upper right panel).

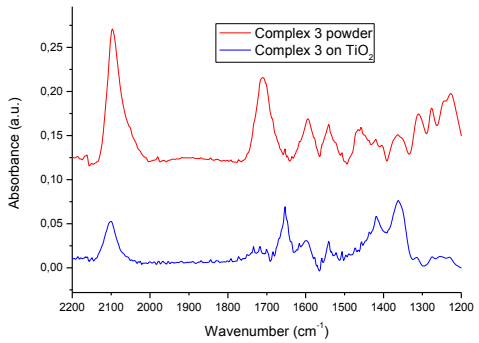

Figure 8. Comparison between the ATR spectrum of Complex **3** powder (red line) and the ATR spectrum of Complex 3 absorbed on TiO_2 (blu line).

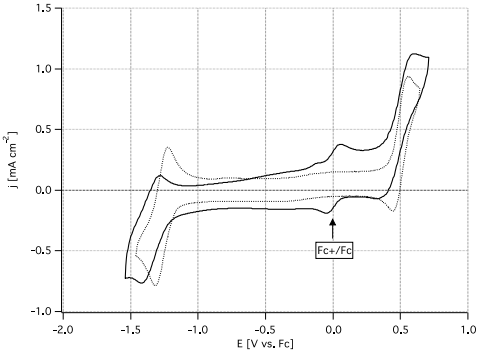

Figure 9. CV of complexes **3** (with Ferrocene added as internal standard) and complex **2** carried out at 1V/s on a glassy carbon electrode, 2nd scan is showed.

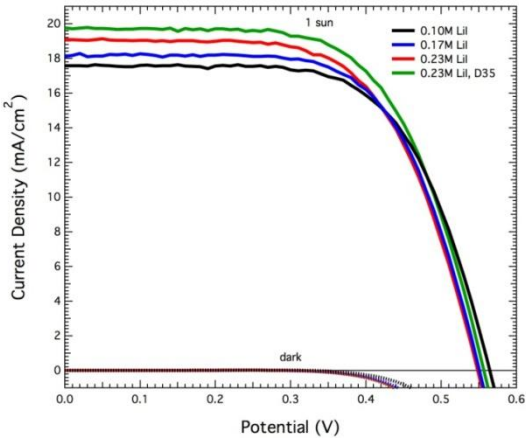

Figure 10. Photovoltaic data of complex **3** as a function of LiI concentration and in the presence of co-sensitization by D35. Dotted lines indicate dark currents of devices.

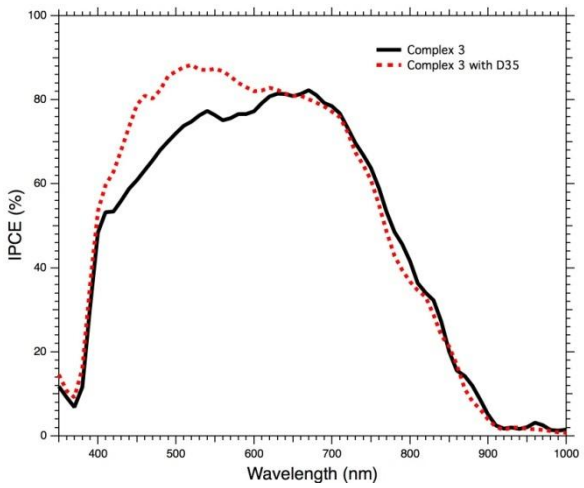

Figure 11. IPCE spectra of DSSCs based on complex **3** without (black solid line) and with D35 (red dashed line). LiI 0.23 M.

TOC graphics